CHAPTER 5

Comparison of graphene oxide based hybrid composite system, and their use as supercapacitor electrodes

5.1. Introduction

In the previous chapter (chapter 4), it has been observed that GO/PANI/$CuCo_2O_4$ based ternary composite exhibited outstanding electrochemical performances than the single and binary systems. In this chapter the focus is on the different ternary composite of graphene oxide-polyaniline-copper ferrite (GO/PANI/$CuFe_2O_4$), graphene oxide-polyaniline-cobalt ferrite (GO/PANI/$CoFe_2O_4$) and compared its structural properties and electrochemical properties with the graphene oxide-polyaniline-copper cobaltite (GO/PANI/$CuCo_2O_4$). The experimental details have been provided in sections 3.2.1 to 3.2.5.

5.2. Results and discussion

5.2.1. XRD

The XRD spectrum of the different ternary prepared materials such as GO/PANI/$CuCo_2O_4$, GO/PANI/$CuFe_2O_4$, and GO/PANI/$CoFe_2O_4$ are shown in figure 5.1. The ternary composite of GO/PANI/$CuCo_2O_4$ consists of peaks at 20.56° (020), 25.25° (200), 31.90° (220), 36.79° (311), 42.72° (110), 44.65° (400), 59.30° (511) and 65.06° (440) as shown in table 4.1. The slight shifting of the characteristic peaks is mainly due to the increase and decrease of the crystallite sizes of the GO, PANI, and $CuCo_2O_4$. The intense peak of GO at 11.05° (001) could not be seen in the GO/PANI and GO/PANI/$CuCo_2O_4$ composite due to the interaction between the individual materials and folding of the disordered chain of polyaniline.

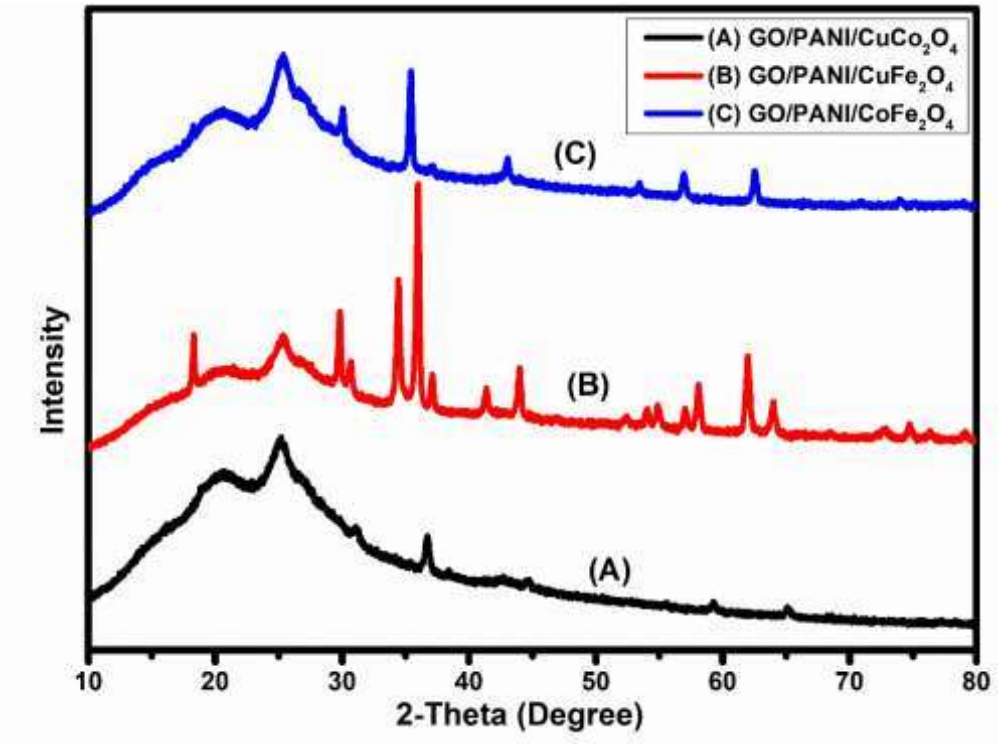

Figure 5.1: XRD pattern of all ternary synthesized materials

The three main peaks in GO/PANI/$CuFe_2O_4$ at 14.79° (011), 20.54° (020), and 25.31° (200) confirmed the presence of polyaniline but the characteristic peak of GO was not seen properly due to the wrapping of periodically arranged semi-crystalline PANI over GO. For GO/PANI/$CuFe_2O_4$, diffraction peaks located at 18.35° (101), 29.73° (112), 30.68° (200), 34.38° (103), 35.96° (211), 36.99° (202), 41.24° (004), 43.98° (220), 54.12° (312), 55.01° (105), 56.99° (303), 58.10° (321), 61.92° (224), 63.99° (400), 72.89° (420), 74.82° (413), and 79.06° (404) are the peaks of $CuFe_2O_4$ (JCPDS 34-0425) and also having PANI peaks such as 20.54° (020) and 25.31° (200). In the case of ternary composite GO/PANI/$CuFe_2O_4$, all the characteristic peaks of $CuFe_2O_4$, as well as PANI, but the characteristic peaks of GO are not seen as GO sheets are covered by the untidy chain of PANI and $CuFe_2O_4$ particles as

shown in table 5.1. These plots along with the JCPDS file confirm the successful synthesis of ternary composite GO/PANI/$CuFe_2O_4$.

Table 5.1: Peak and hkl values of GO/PANI/$CuFe_2O_4$

Peaks	Diffraction angle (in degree)	hkl
1	14.79	011
2	18.35	101
3	20.54	020
4	25.31	200
5	29.73	112
6	30.68	200
7	34.38	103
8	35.96	211
9	36.99	202
10	41.24	004
11	43.98	220
12	54.12	312
13	55.01	105
14	56.99	303
15	58.10	321
16	61.92	224
17	63.99	400
18	72.89	420

19	74.82	413
20	79.06	404

The ternary GO/PANI/$CoFe_2O_4$ having peaks around 14.85° (011), 18.31° (111), 20.39° (020), 25.24° (200), 30.11° (220), 35.59° (311), 37.12° (222), 42.98° (400), 53.43° (422), 56.98° (511), 62.56° (440), 74.03° (533), 75.04° (622), 79° (444) provide the confirmation of GO, PANI, and $CoFe_2O_4$ [JCPDS 22-1086] in ternary system as shown in table 5.2.

Table 5.2: Peak and hkl values of GO/PANI/$CoFe_2O_4$

Peaks	**Diffraction angle (in degree)**	**hkl**
1	14.85	011
2	18.31	111
3	20.39	020
4	25.24	200
5	30.11	220
6	35.59	311
7	37.12	222
8	42.98	400
9	53.43	422
10	56.98	511
11	62.56	440
12	74.03	533
13	75.04	622

14	79.00	444

Furthermore, XRD analysis was also used to find out the interlayer spacing (d) and crystalline size (L) with the help of Bragg's and Scherrer's equation (equations 4.1 and 3.4) as shown in table 5.3.

Table 5.3: Peak assignments of all ternary prepared materials

Sample	d (nm)	FWHM (degree)	L (nm)
GO/PANI/$CuCo_2O_4$	0.24	0.39	22.31
GO/PANI/$CuFe_2O_4$	0.25	0.26	31.40
GO/PANI/$CoFe_2O_4$	0.25	0.29	28.75

The prime parameters such as interlayer spacing (d) and crystalline size (L) of different ternary synthesized materials are given in table 5.3. The interlayer spacing (d) is highest for GO/PANI/$CuFe_2O_4$ and GO/PANI/$CoFe_2O_4$ but lesser for ternary GO/PANI/$CuCo_2O_4$ which is mainly due to the distortion of PANI chain and some intercalated oxygen functional groups reduction. The functional groups formed the π-bond conjugate system over GO surface. It was found that crystallite sizes (L) for GO/PANI/$CuCo_2O_4$, GO/PANI/$CuFe_2O_4$, and GO/PANI/$CoFe_2O_4$ were 22.31 nm, 31.40 nm, and 28.75 nm, respectively. The increment and decrement in the crystalline size (L) may be due to the degree of reduction and oxidation of materials.

5.2.2. FTIR

Figure 5.2 demonstrates the Fourier transform infrared (FTIR) spectrum of all prepared ternary samples such as GO/PANI/$CuCo_2O_4$, GO/PANI/$CuFe_2O_4$, and GO/PANI/$CoFe_2O_4$ for investigation of the various functional groups. The absorption peaks in all ternary were attributed to 3394 cm^{-1}, 2911 cm^{-1}, 1623 cm^{-1}, and 1038 cm^{-1}, which were assigned to the O-H groups stretching, aliphatic stretching of C-H groups, bending of O-H groups, and C-O vibrational stretching [215]. The spectroscopically bands at 1570 cm^{-1} and 1484 cm^{-1} attributed to the stretching vibrations of C=C based on quinone and benzene rings in polyaniline. The peaks at 1301 cm^{-1} can correspond to C-N stretching vibrations in the polyaniline quinoid ring, and the peak at 1113 cm^{-1} can be assigned to the N=Q=N stretching vibration. The peak at 813 cm^{-1} corresponds to the deformation of C-H groups, and at 620 cm^{-1} can be located as an unsymmetrical stretching of the S-O group, which is existing in PTSA-PANI [29,210]. For $CuCo_2O_4$, peaks at 567 cm^{-1} for Co-O and 663 cm^{-1} due to Cu-O [211,212]. Similarly, the existence of $CuFe_2O_4$ can be proven by the small peaks at 553 cm^{-1} for Cu-O and at 443 cm^{-1} for Fe-O, which are also present in the curve for PANI/$CuFe_2O_4$ and GO/PANI/$CuFe_2O_4$ [216,217]. For $CoFe_2O_4$, bands at 567 cm^{-1} for Fe-O and 673 cm^{-1} due to Co-O [218,219]. The spike at 3394 cm^{-1} in all ternary is smoother and wider, which corresponds to the depletion of hydroxyl and carboxyl groups during the time of composite formation. Furthermore, the little peak variation of PANI and different metal oxides in composite due to the chemical interaction and interrelation with GO might be responsible for the delocalization of charges in the backbone of polyaniline.

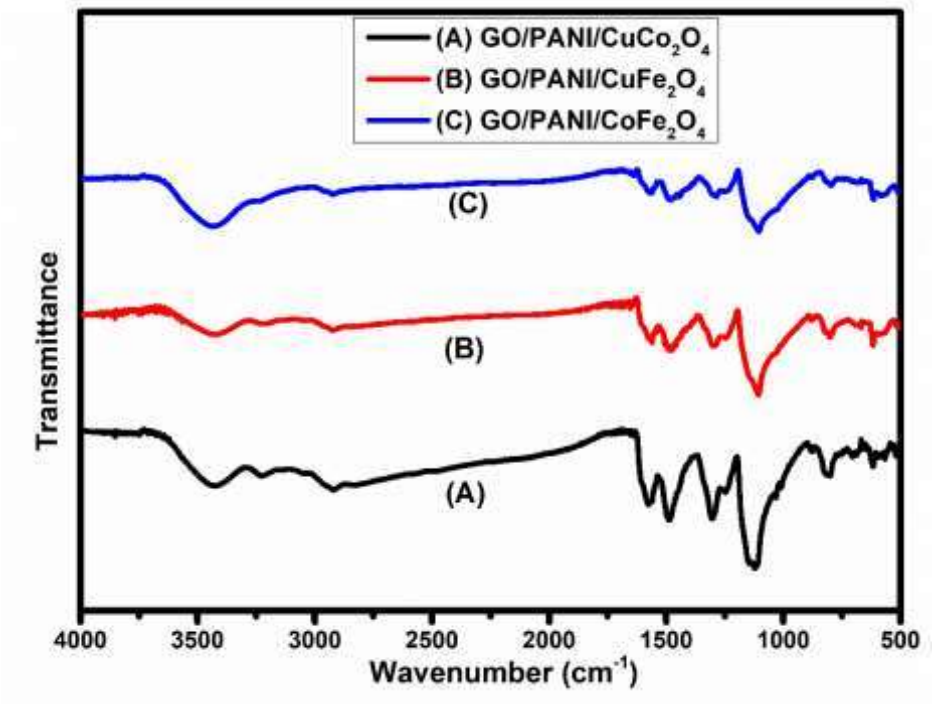

Figure 5.2: FTIR pattern of all ternary synthesized materials

5.2.3. FE-SEM

The surface morphology of the synthesized materials was identified with the help of FESEM and displayed in figure 5.3. In GO/PANI/$CuCo_2O_4$, the $CuCo_2O_4$ particles may have dispersed into the polyaniline rod-like structure. Due to this, the polyhedral texture of $CuCo_2O_4$ does not look in the PANI/$CuCo_2O_4$, and only rod-like shapes with an agglomeration of PANI particles are noticed. In the ternary GO/PANI/$CuFe_2O_4$ composite, the polyaniline chain may have been well distributed and scattered onto the layers of GO, hence it appears to be a rod-like structure. Furthermore, the particles of $CuFe_2O_4$ may have well dispersed into the rods of PANI. So, the complete visualization of $CuFe_2O_4$ particles has not been seen properly and is seen in majorly PANI rod-like agglomeration structures. In GO/PANI/$CoFe_2O_4$, PANI and $CoFe_2O_4$ particles would have been dispersed in GO, which can be observed from figure 5.3 (C). The micelle structure might be changed due to

the addition of sonicated different metal oxides and GO in ternary composite, which assembled at the time of aniline addition in PTSA mixture.

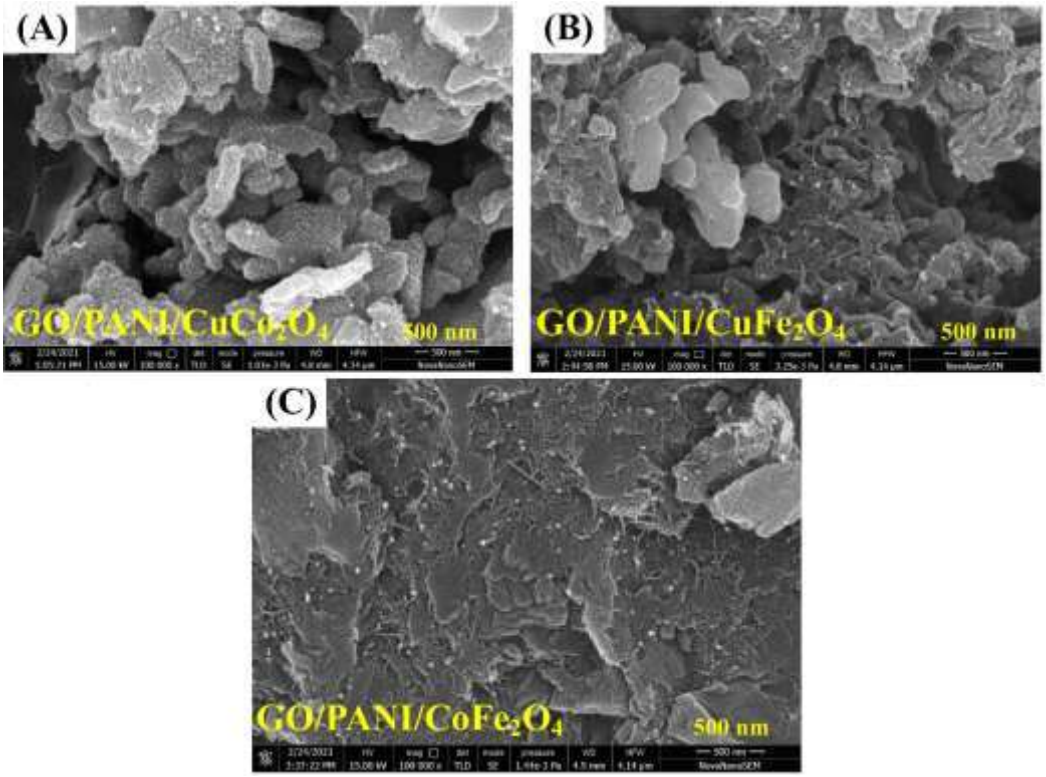

Figure 5.3: FE-SEM pictures of different ternary composite

5.2.4. Elemental analysis from the morphology

All the elemental information such as composition in terms of weight % and atomic % is shown in figure 5.4. The table provided within EDS spectrum easily indicated that Cu:Co, Cu:Fe, and Co:Fe proportion in the composites is approximately equal to the composition which was taken during the composites synthesis.

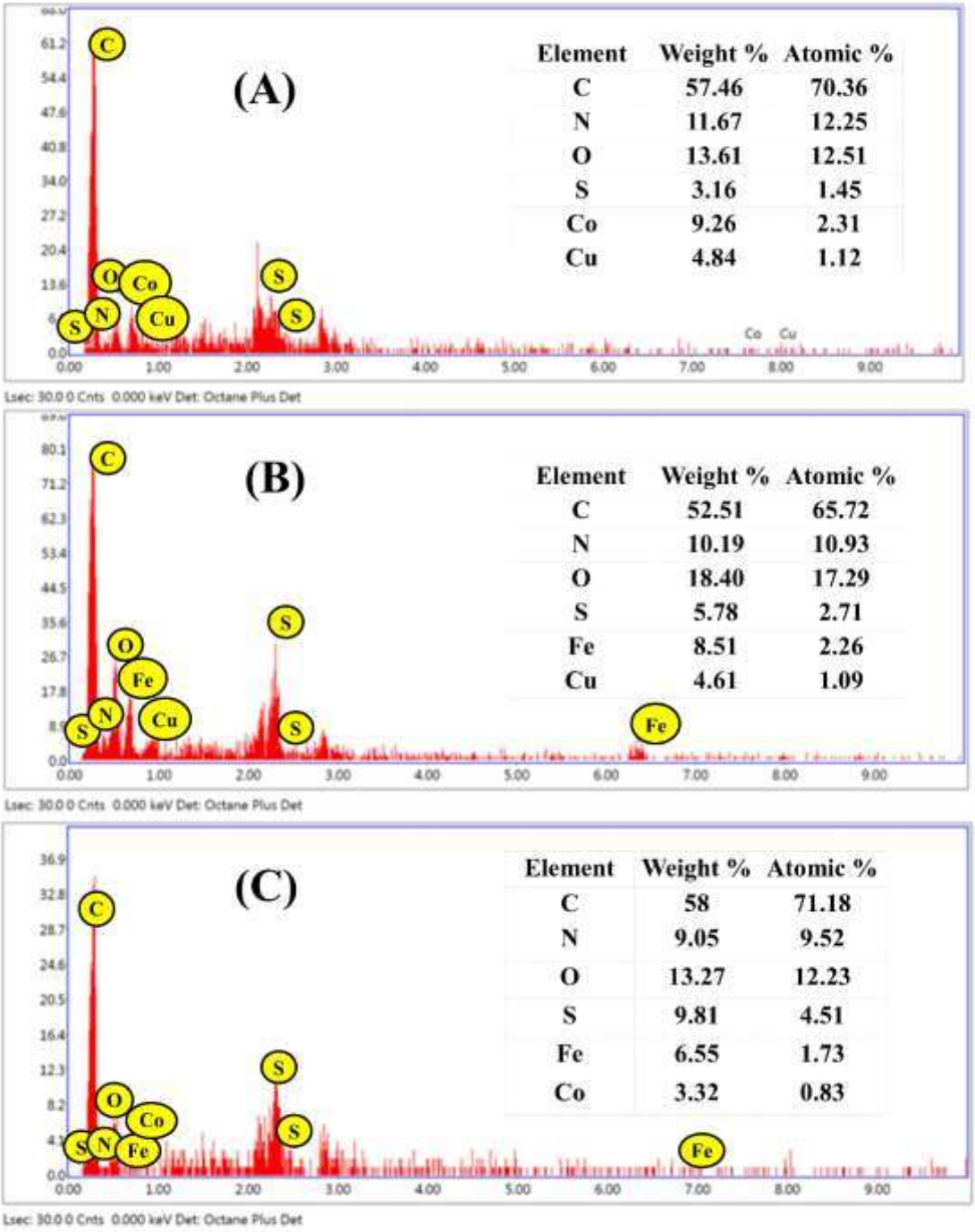

Figure 5.4: EDS spectrum of (A) GO/PANI/$CuCo_2O_4$; (B) GO/PANI/$CuFe_2O_4$; (C) GO/PANI/$CoFe_2O_4$

5.2.5. Elemental mapping

The elemental EDS mapping of synthesized samples has been displayed in figure 5.5. From the elemental mapping images, we can notice that all the components have uniform distribution with respective proportions in the composite. It proves that the composite is successfully formed.

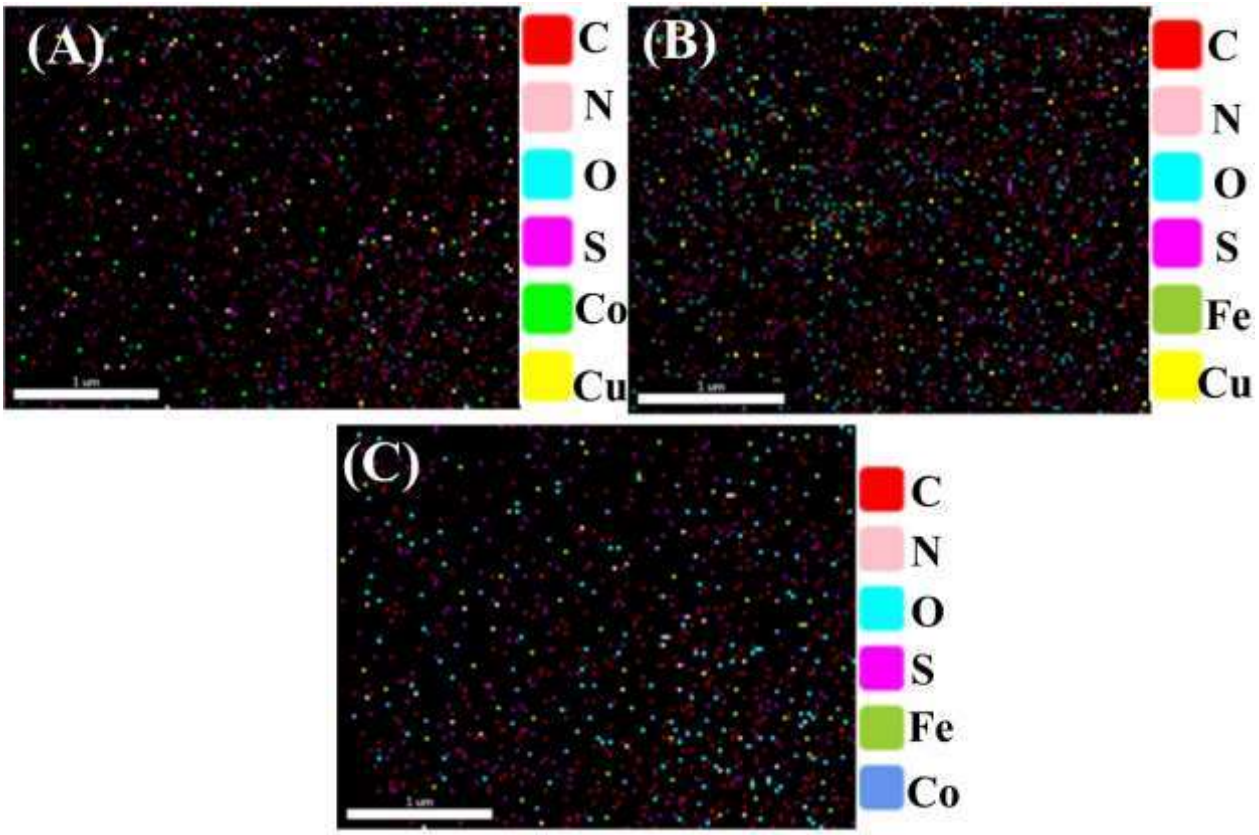

Figure 5.5: Elemental EDS mapping spectrum of (A) GO/PANI/$CuCo_2O_4$; (B) GO/PANI/$CuFe_2O_4$; (C) GO/PANI/$CoFe_2O_4$

5.2.6. Electro-chemical nature

The electro-chemical behavior of all synthesized ternary materials has been evaluated from CV (cyclic voltammetry) and CD (charge-discharge). The CV (cyclic voltammetry) curve of different ternary synthesized material electrodes using 3E (three-electrode) at scan rate of 1

mV/s is shown in figure 5.6 (A). CV plot of GO/PANI/$CuCo_2O_4$, GO/PANI/$CuFe_2O_4$, and GO/PANI/$CoFe_2O_4$

also have been discussed at various scan rates such as 1, 2, 5, 10, and 20 mV/s and shown in figure 5.6 (B-D). Some materials show their property in the negative potential window and some show in the positive potential range. So, it is necessary to scan the samples in between higher and lower potential to find out the electrochemical behavior of the materials. CV was done to find out the stability potential window and that window had been incorporated in CD.

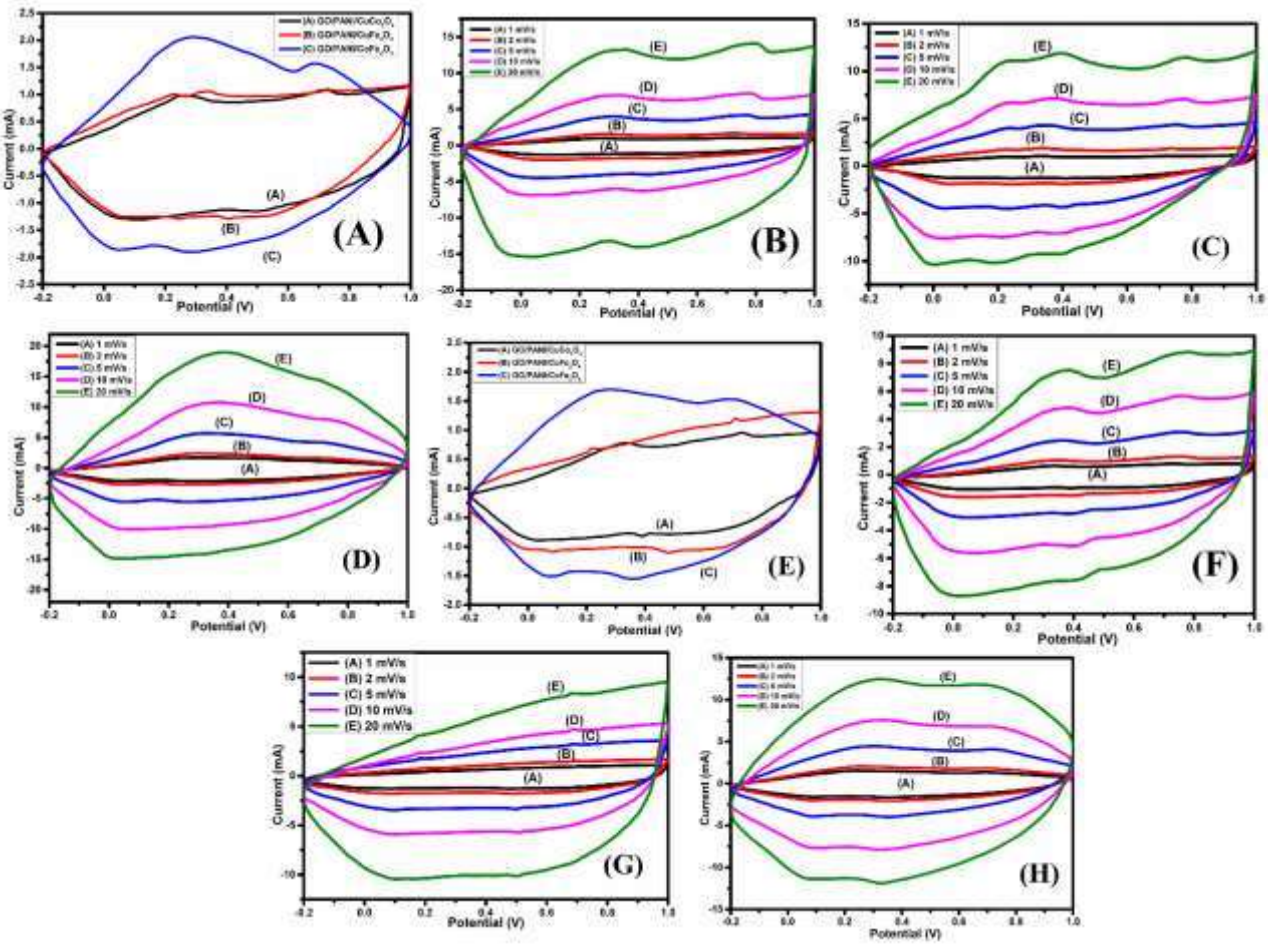

Figure 5.6: CV (Cyclic voltammetry) plot of different ternary synthesized materials at (A) Scan rate of 1 mV/s using the 3E system; (B) Distinct scan rates using the 3E system for GO/PANI/$CuCo_2O_4$; (C) Distinct scan rates using the 3E system for GO/PANI/$CuFe_2O_4$; (D) Distinct scan rates using the 3E system for GO/PANI/$CoFe_2O_4$;

(E) 1 mV/s using the symmetric 2E system of different ternary; (F) Distinct scan rates using the symmetric 2E system for GO/PANI/$CuCo_2O_4$; (G) Distinct scan rates using the symmetric 2E system for GO/PANI/$CuFe_2O_4$; (H) Distinct scan rates using the symmetric 2E system for GO/PANI/$CoFe_2O_4$

GO has a carbon-based material and shows the almost rectangular type CV curve which is mainly due to the EDLC (electric double layer capacitive) behavior of material. While all ternary showed some oxidation and reduction peaks and showed the pseudocapacitive nature because of PANI and different metal oxides. The CV curve of all three ternary demonstrates the integral nature of pseudocapacitive and EDLC. Normally, there are mainly three oxidation-reduction peaks of pure PANI (polyaniline) located at 0.28 V, 0.57 V, 0.72 V corresponding to oxidation and 0.03 V, 0.41 V, 0.63 V denoting the reduction states. Peak around 0.28 V oxidation is mainly because of leucoemeraldine conversion into emeraldine salt and oxidation at 0.57 V denoted as hydroquinone/benzoquinone degradation state. A spike at 0.72 V is due to emeraldine to pernigraniline conversion [220]. The oxidation peaks at 0.3 V and 0.4 V are corresponding to the Co^{3+}/Co^{4+} and Cu^{2+}/Cu^{3+} transition of $CuCo_2O_4$ in ternary GO/PANI/$CuCo_2O_4$ [214]. For the ternary GO/PANI/$CuCo_2O_4$, the oxidation peak at around 0.58 V disappeared, which could be mainly due to the involvement of GO and $CuCo_2O_4$ particles [207]. The oxidation peaks of $CuCo_2O_4$ are not seen in ternary GO/PANI/$CuCo_2O_4$ because metal oxides (i.e. $CuCo_2O_4$) have high density and graphene

oxide possesses of high surface area. The metal oxide may be dispersed into the graphene oxide pores and the surface of metal oxide and graphene oxide may be covered with PANI structure.

On the other hand, the oxidation peaks at 0.32 V and 0.71 V correspond to the Cu^{2+}/Cu^{3+} and Fe^{2+}/Fe^{3+} transitions of $CuFe_2O_4$ in ternary GO/PANI/$CuFe_2O_4$. For GO/PANI/$CuFe_2O_4$, the 0.57 V oxidation peak was not properly visible, this was mainly because of the incorporation of GO and $CuFe_2O_4$ particles. Oxidations at 0.34 V and 0.32 V were shown for GO/PANI/$CuFe_2O_4$ due to the insertion of $CuFe_2O_4$ and these peaks were allocated to the transition of Cu^{2+}/Cu^{3+}. The location of the 0.7 V oxidation peak in GO/PANI/$CuFe_2O_4$, is mainly due to Fe^{2+}/Fe^{3+} and emeraldine salt/pernigraniline transition.

The peaks at 0.24 V and 0.63 V oxidation due to the Co^{2+}/Co^{3+}, Co^{3+}/Co^{4+} and Fe^{6+}/Fe^{3+} transitions of $CoFe_2O_4$ in ternary GO/PANI/$CoFe_2O_4$. $CoFe_2O_4$ go through the following electrochemical reactions.

$$CoFe_2O_4 + H_2O + OH^- \leftrightarrow 2FeOOH + CoOOH + e^-$$

(5.1)

$$CoOOH + OH^- \leftrightarrow CoO_2 + H_2O + e^-$$

(5.2)

$$FeOOH + H_2O \leftrightarrow Fe(OH)_3 \leftrightarrow (FeO_4)^{2-} + 3e^-$$

(5.3)

The CV curve for all ternary at various scan rates is also given in figure 5.6 (B-D) and indicated that peak current value and voltammetric area increase as the scan rate increases. Here the maximum peak current value is due to the merged effect of faradaic and capacitive

current. As the scan rate is increasing, the interaction time between the active material electrode and electrolyte ions is very low. Due to the less interaction, the probable redox transitions are not occurring and the specific capacitance is decreased. The overall value of the capacitance is due to combined behaviour of EDLC and pseudocapacitance, but as scan rate increases, the pseudocapacitance contribution decreases. Equation 4.5 to 4.7 were used to find out the values of specific capacitance (C_s) from the 3E CV, 2E CV, and symmetric 2E CD.

Similarly, all ternary composite has shown CV curve using a symmetric 2E system as shown in figure 5.6 (E). The integral nature of PANI, different metal oxides (pseudocapacitive), and GO (EDLC) material shows the various oxidation-reduction (redox) reactions. The maximum voltammetric area and large value of peak current are mainly due to the high mobility of ions in all ternary composites. So, ternary hybrid composite shows the maximum specific capacitance compared to others. Furthermore, the variation of scan rates in the voltammetric area for ternary composite shown in figure 5.6 (F-H), and concluded that voltammetric area is increases with scan rate. Due to larger area, the peak current also grows up, while capacitance values decrease due to less duration of active electrode surface and electrolyte interaction. The values of different capacitances with increasing scan rates using 3E and symmetric 2E systems are shown on table 5.4.

Table 5.4: Different values using 3E and symmetric 2E systems

Material	Scan rate	CV 3E	CV 2E	Current	CD 2E	Esp (Wh/kg)	Psp (W/kg)

	(mV/s)	C_s (F/g)	C_s (F/g)	density (A/g)	C_s (F/g)		
GO/PANI/$CuCo_2O_4$	1	741.39	308.15	1	312.72	62.54	300.04
GO/PANI/$CuFe_2O_4$	1	790.12	318.26	1	357.28	71.45	300.03
GO/PANI/$CoFe_2O_4$	1	781.27	305.14	1	346.92	69.38	300.08
GO/PANI/$CuCo_2O_4$	2	679.48	261.12	2	286.07	57.21	598.92
GO/PANI/$CuCo_2O_4$	5	602.08	214.52	5	261.44	52.28	1497.11
GO/PANI/$CuCo_2O_4$	10	518.93	179.36	10	233.67	46.73	30006.50
GO/PANI/$CuCo_2O_4$	20	445.16	153.44	20	208.83	41.76	5997.61
GO/PANI/$CuFe_2O_4$	2	695.54	278.46	2	310.89	62.17	602.13
GO/PANI/$CuFe_2O_4$	5	611.02	231.78	5	266.25	53.25	1503.20
GO/PANI/$CuFe_2O_4$	10	512.81	191.62	10	238.60	47.72	3010.70

GO/PANI/$CuFe_2O_4$	20	382.65	161.16	20	214.29	42.85	5983.90
GO/PANI/$CoFe_2O_4$	2	672.48	251.24	2	304.06	60.81	601.12
GO/PANI/$CoFe_2O_4$	5	602.36	214.57	5	259.09	51.83	1502.61
GO/PANI/$CoFe_2O_4$	10	497.85	175.48	10	230.12	46.02	3008.18
GO/PANI/$CoFe_2O_4$	20	362.81	168.47	20	204.14	40.82	5989.37

Figure 5.7 (A) shows the CD behavior of different ternary synthesized materials using a symmetric 2E system at a constant 1 A/g current density. Ternary GO/PANI/$CuFe_2O_4$ composite showed a large charge and discharge time than other materials, and the high charge and discharge time of ternary is responsible for the maximum value of capacitance as well known that specific capacitance value directly depends upon discharge time. Similarly, the changes of charge and discharge time with different current densities for all ternary shown in figure 5.7 (B-D), and realized that charge and discharge time decreases with current density increases from 1 A/g to 20 A/g. So, the lowest specific capacitance value was found at the current density of 20 A/g and the highest at the current density of 1 A/g for all systems. In the CD plot, the curves are not completely triangular (distorted) in shape, which could be due to the pseudocapacitive materials like PANI and different metal oxides. Negligible ohmic loss (IR drop) was observed suggesting outstanding reversibility of the

system. Table 5.4 gives different specific capacitance values using a CD plot. At high current density, the inactive sites of electrode material develop the ion diffusion barrier, so a lower specific capacitance value is obtained [221].

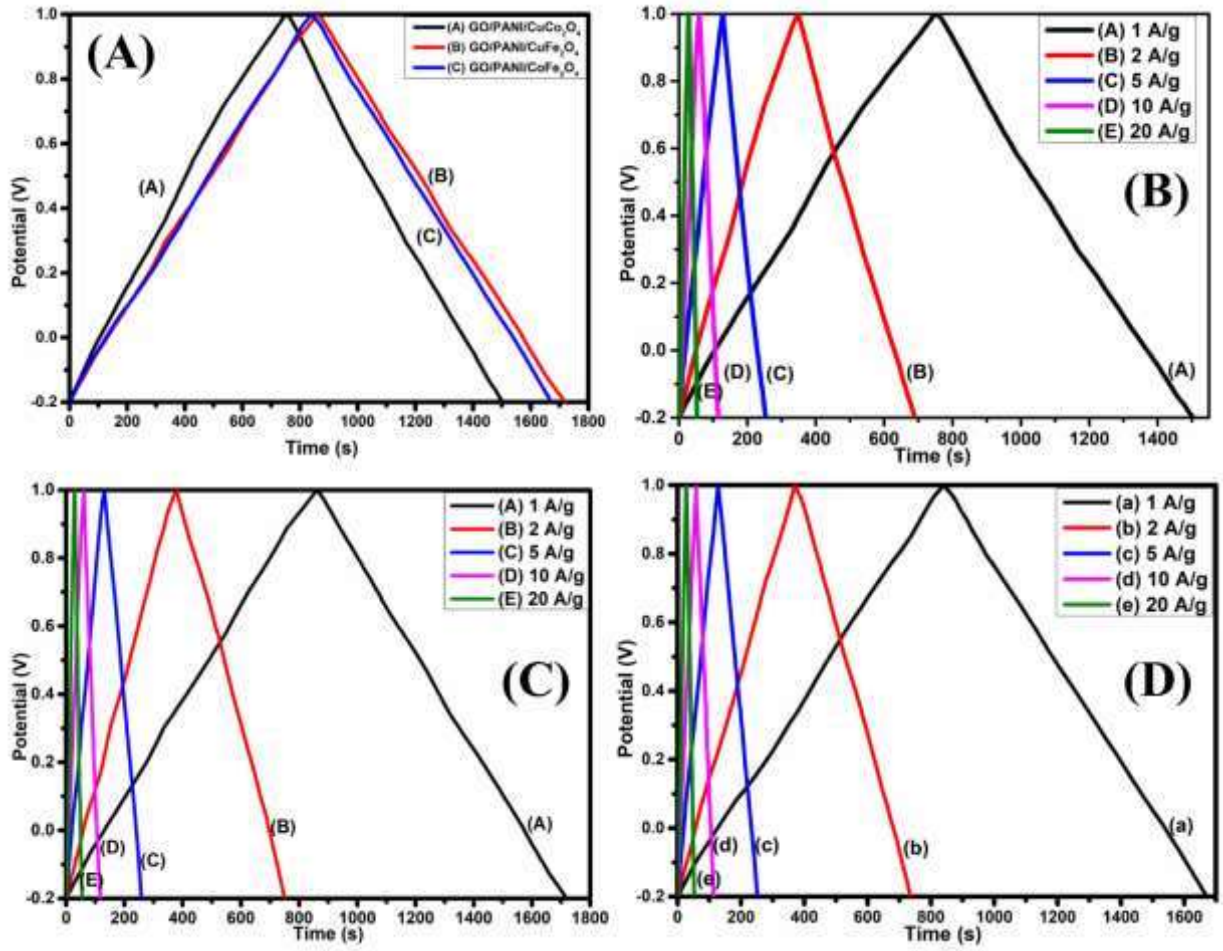

Figure 5.7: Charge-discharge (CD) curve (A) At 1 A/g of different ternary, (B) For ternary GO/PANI/$CuCo_2O_4$ with current density variation, (C) For ternary GO/PANI/$CuFe_2O_4$ with current density variation, (D) For ternary GO/PANI/$CoFe_2O_4$ with current density variation

There are also two main parameters that define the performance of supercapacitor material. The specific power defines the charge deliver capability, whereas specific energy is the capacity of storing charges. Equations 4.8 and 4.9 were used to find out the respective values.

Furthermore, the variation of Psp and Esp (Ragone plot) of different synthesized materials is displayed in figure 5.8 (A). Ternary GO/PANI/$CuFe_2O_4$ composite shows a high value of specific energy compared to other prepared materials. Table 5.4 provides the values of specific power and specific energy for different electrode materials, and concluded that GO/PANI/CuFe2O4 has a high specific energy than others. But the specific power of different samples is almost the same at 1 A/g, which shows that all materials have the same ability to convey the charge that is stored inside them. Different values of Esp and Psp are calculated at various current densities, and it is observed that the Esp value continuously decreases and the Psp value constantly increases from 1 A/g to 20 A/g current density.

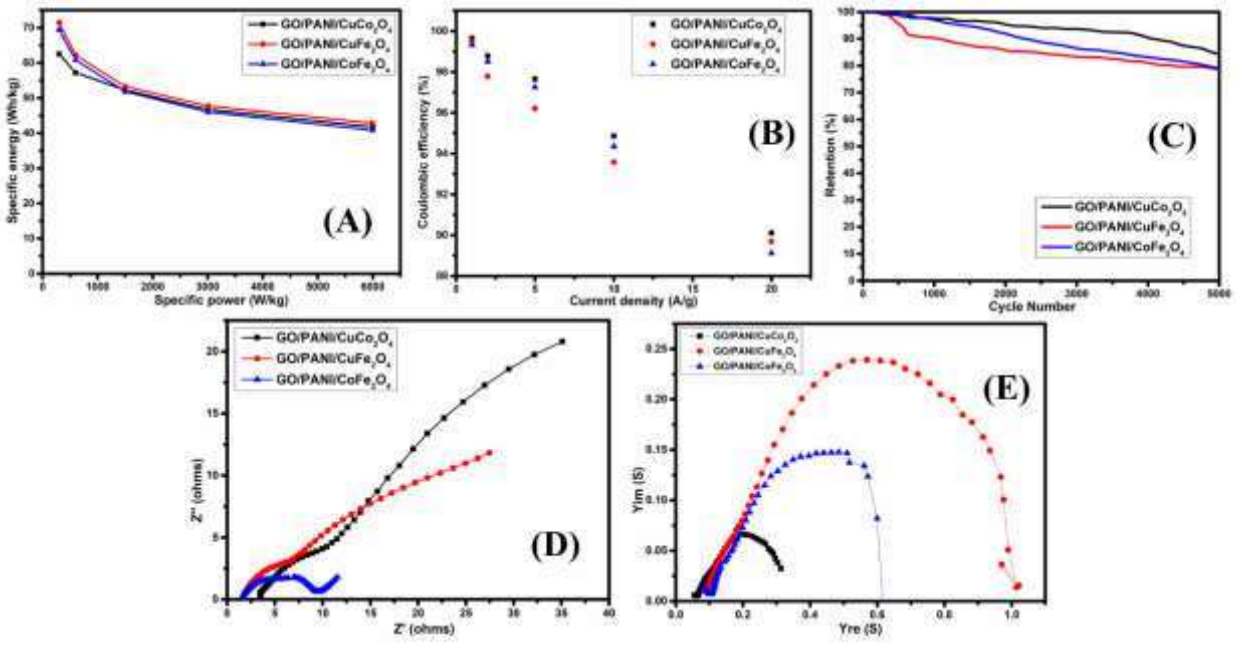

Figure 5.8: (A) Ragone plot, (B) Coulombic efficiency vs current density, (C) Retention (%) vs number of cycle, (D) EIS plot, (F) Yre vs Yim

The ability of charge conveying is defined by the coulombic efficiency and its values for different materials have been calculated by using symmetric charge and discharge time according to equation 4.10.

Figure 5.8 (B) shows the changes in coulombic efficiency (%) with current density (A/g) and summarizes that value of coulombic efficiency (%) decreases as current density increases. The decrease could be because of irreversible behaviour during charge-discharge and high polarization. GO/PANI/$CuCo_2O_4$ composite showed high value of coulombic efficiency of 90.11 % at 20 A/g current density. Furthermore, the cyclic stability of prepared materials was also analyzed up to 5000 CV cycles at 100 mV/s scan rate and still 84.25 % capacitance retention was observed after 5000 cycles for ternary GO/PANI/$CuCo_2O_4$ composite (Figure 5.8 (C)). The capacitance loss is mainly due to less interaction between the electrode and electrolyte. It is well-known that different metal oxides and PANI-type materials have shown low cyclic stability due to inappropriate volume contraction expansion and diminished performance during charging-discharging. With the addition of pristine GO in PANI and different metal oxides composite, the cyclic stability of the formed ternary grown up. And also GO acts as a backbone support for both PANI and different metal oxides, hence restricting the damage on the surface.

To analyze the electrochemical nature of the synthesized electrode materials on the interface between electrolyte-electrode, EIS was completed in 1M KOH aqueous electrolyte to evaluate the different resistance like Rs, Rct, diffusion resistance or Warburg impedance (w), and capacitive behaviour of the synthesized material (figure 5.8 (D)). The intercept in the x-

axis after plotted quasi semicircle is defined as Rs and the diameter of plotted semicircle is Rct. Basically, Rs is due to the combined resistance of the material, and electrolyte solution. From table 5.5, ternary GO/PANI/$CuFe_2O_4$ has shown a lower Rs value than other samples while ternary GO/PANI/$CoFe_2O_4$ has displayed a lower Rct value, which could be because of more active sites in material and the easy transportation of ions. This smooth diffusion of ions is mentioned by the good electrode and electrolyte interaction and large number of active places in GO/PANI/$CoFe_2O_4$ which favored the good penetration of ions on the GO/PANI/$CoFe_2O_4$. In general, metal oxide shows less electrical conductivity due to the presence of internal voids. But the addition of GO and PANI may help in providing proper electrical connection and therefore, the overall electrochemical performance of the system may get enhanced.

Table 5.5: R_s and R_{ct} values of synthesized ternary materials

Material	R_s (Ω)	R_{ct} (Ω)
GO/PANI/$CuCo_2O_4$	3.25	12.23
GO/PANI/$CuFe_2O_4$	1.40	8.72
GO/PANI/$CoFe_2O_4$	1.61	8.51

Figure 5.8 (E) gives the changes of admittance between the imaginary and real axis to evaluate the response time (t_r) of different samples. The readiness of the system during the electrochemical reactions can be obtained from the response time (t_r) given by equation 4.11 [222].

The information about the utilization of charges stored in a system can be obtained from the knee frequency (f_k). Table 5.6 shown the different values of response times (t_r) and knee frequencies (f_k) of various samples.

Table 5.6: f_k and t_r values of synthesized electrode materials

Material	f_k (Hz)	t_r (ms)
GO/PANI/$CuCo_2O_4$	1.58	632.91
GO/PANI/$CuFe_2O_4$	6.30	158.73
GO/PANI/$CoFe_2O_4$	3.16	316.45

GO/PANI/$CuFe_2O_4$ has a low value of response time (tr) due to a large portion of EDLC behaviour and only the presence of physical adsorption. In the case of ternary GO/PANI/$CuCo_2O_4$ composite, tr value is very large compared to other samples just mainly due to a greater number of oxidation-reduction reactions going on the electrode-electrolyte interface. So, the competition of these several oxidation-reduction reactions took much more time than other prepared samples.

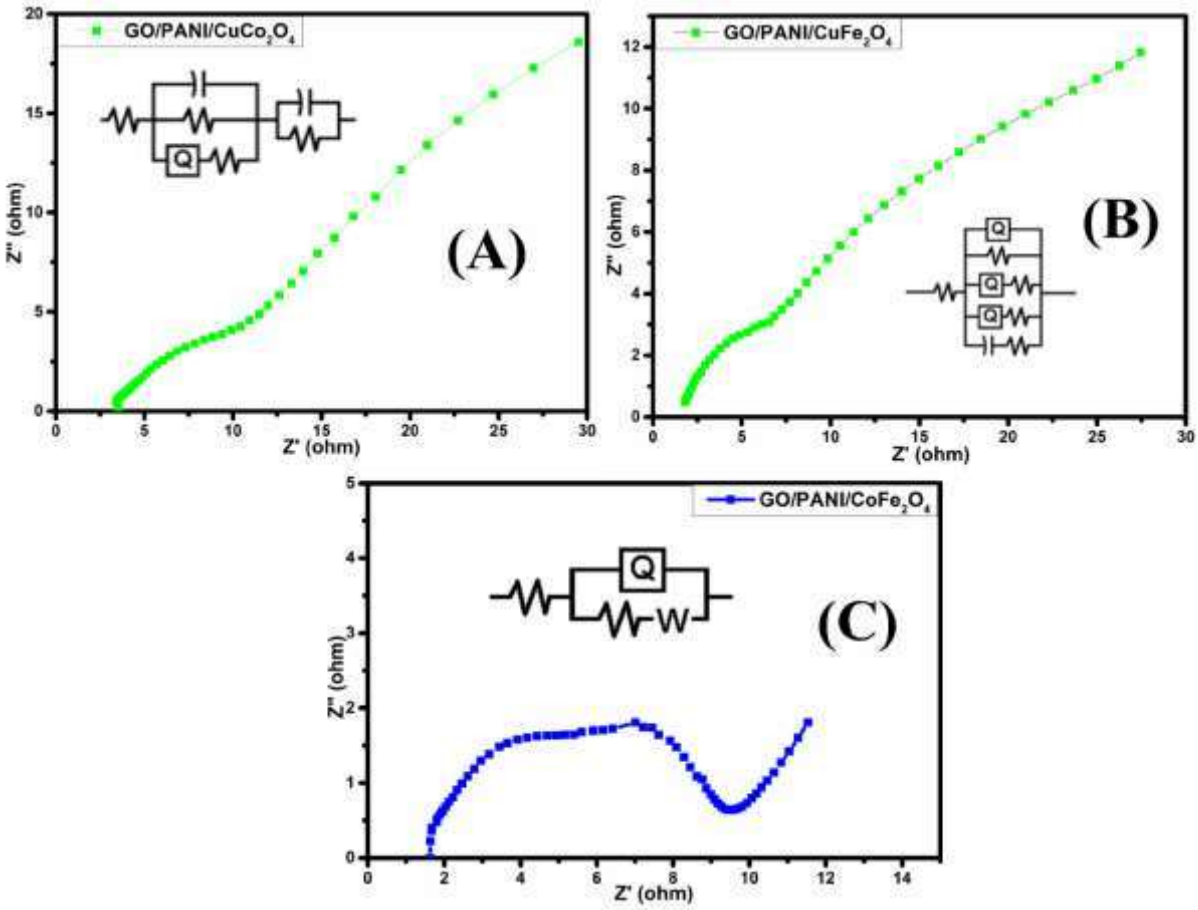

Figure 5.9: Equivalent circuit diagrams from Nyquist plot

The equivalent circuit diagrams corresponding to the different prepared systems have been shown in figure 5.9. The different equivalent circuits for all prepared samples could be due to the different internal mechanisms of ion transportation during charging-discharging. There are many types of resistance present in all synthesized samples including capacitance due to the two types of capacitance such as EDLCs and pseudocapacitance, constant phase element (Q) which shows the non-ideality of the supercapacitor due to the interface film resistance and some electrolyte barriers.

The different specific capacitance values of different metal oxide based materials are shown in table 5.7. It was seen that GO/PANI/$CuFe_2O_4$ ternary had a higher value of specific

capacitance compared to others ternary materials due to the better interaction of GO and $CuFe_2O_4$ particles in PANI during synthesis. Here GO has restricted the excessive contraction-expansion of PANI and offers the higher stability with enhanced electrochemical performance.

Table 5.7: Comparison of the specific capacitance of some related electrode material in the literature

Sample	Electrolyte	Potential window (V)	Scan rate (mV/s)/ Current density (A/g)	C_s (F/g)	References
$CuFe_2O_4$-FMWCNT	1 M KCl	-0.3→1	10 mV/s	267	[179]
$CuFe_2O_4$ Film	1 M NaOH	-0.2→0.7	0.3 μA/cm^2	5.7	[223]
$CuFe_2O_4$ Fiber	1 M KOH	-0.1→0.4	0.5 A/g	28	[224]
$CoFe_2O_4$	1 M KOH	-1→0	1	195	[218]
$CoFe_2O_4$	1 M NaOH	-1→-0.2	5	366	[225]
$CoFe_2O_4$	1 M KOH	-0.8→0.2	1	52.5	[226]
$CoFe_2O_4$/Graphene	1 M KOH	-0.8→0.2	1	254.5	[226]
$CoFe_2O_4$/rGO	2 M KOH	0.1→0.55	2	551	[227]
$CoFe_2O_4$/AB/PANI	1 M KOH	-0.2→0.8	5	568.23	[221]

$CuFe_2O_4$ nanosphere	1 M KOH	0→0.4	0.6 A/g	334	[228]
$CuFe_2O_4$-PANI-AB	1 M KOH	-0.2→0.8	5 mV/s	572	[229]
GO/PANI/$CuCo_2O_4$	1 M KOH	-0.2→1	1 mV/s, 1 A/g	741.39 312.72	Our work
GO/PANI/$CuFe_2O_4$	1 M KOH	-0.2→1	1 mV/s, 1 A/g	790.12, 357.28	Our work
GO/PANI/$CoFe_2O_4$	1 M KOH	-0.2→1	1 mV/s, 1 A/g	781.27 346.92	Our work

In the ternary GO/PANI/$CuFe_2O_4$ electrode material, we have got a higher specific capacitance value than other synthesized binary materials. The appearance of GO in ternary GO/PANI/$CuFe_2O_4$ composite largely restricts the volumetric contraction-expansion of PANI molecules. The inclusion of $CuFe_2O_4$ in the prepared ternary composite enhances the charge transmission mechanism. And overall, the ternary system exhibited excellent electrochemical properties due to the synergistic effect.

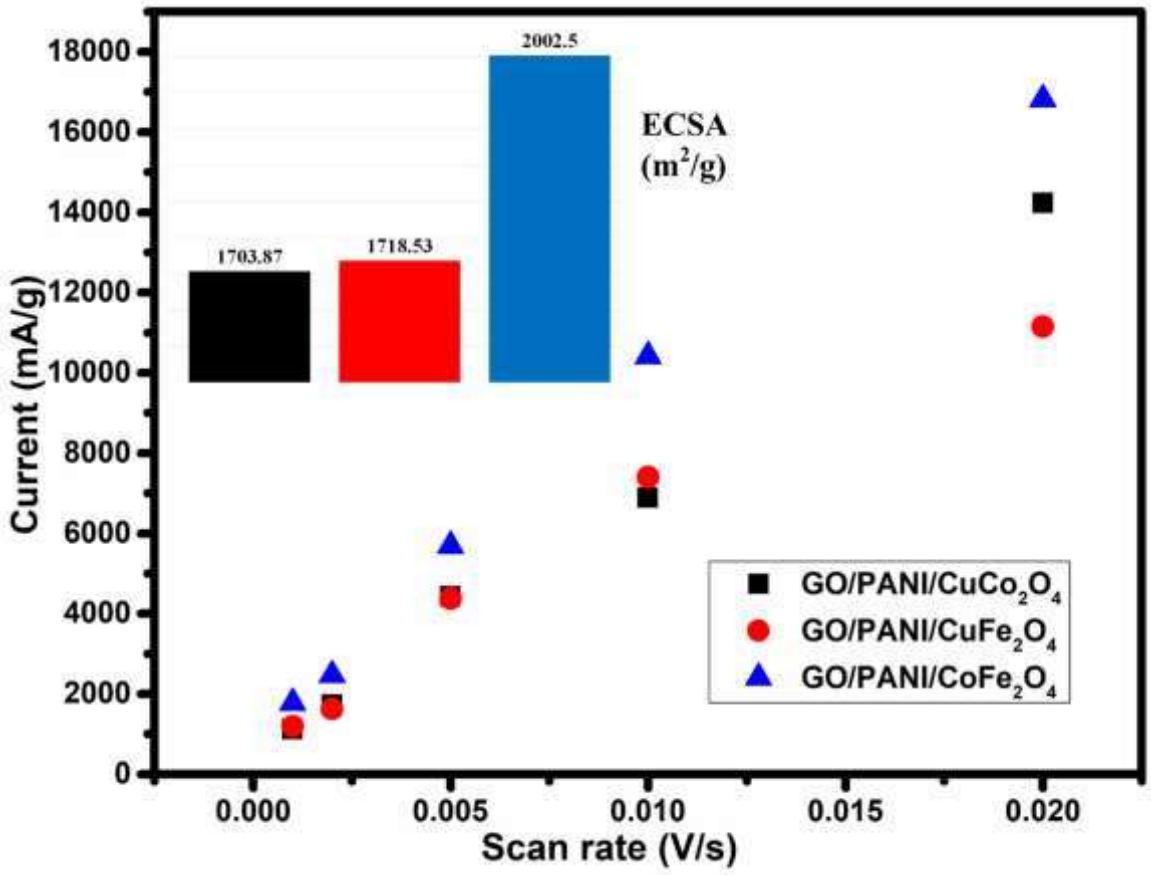

Figure 5.10: ECSA values for different system

The electrochemically active surface area (ECSA) for each system was estimated from the electrochemical double-layer capacitance of the active surface. To know about the electroactive sites on the different composite structure, ECSA of the different composite is further evaluated by double-layer capacitance measurements at the solid-liquid interface through the CV 3E system (figure 5.10). The plot of current density versus scan rate gives a straight line, the slope of this straight line gives the value of C_{dl}. The ECSA is calculated by dividing the C_{dl} by Cs (Cs is the specific capacitance of the sample or the capacitance of an atomically smooth planar surface of the material per unit area under identical electrolyte conditions), which is 0.040 mF/cm^2, and high surface area of 2002.5 m^2/g is

observed for GO/PANI/$CoFe_2O_4$ that is indicative of the larger surface area and more exposed active sites on the interface, which is highly desirable for energy storage application.

5.3. Conclusion

In summary, we have successfully synthesized all ternary composite, in which GO/PANI/$CuFe_2O_4$ exhibited the excellent electrochemical behavior for supercapacitor compare to others synthesized material. The hybrid GO/PANI/$CuFe_2O_4$ composite provides 790.12 F/g at 1 mV/s using 3E system and 357.28 F/g specific capacitance at 1 A/g from symmetric 2E device. The hybrid GO/PANI/$CuFe_2O_4$ composite also given 71.45 Wh/kg specific energy, specific power of 5983.90 W/kg, and 78.77 % capacitance retention after 5000 cycles. The inclusion of GO in PANI/$CuFe_2O_4$ (GO/PANI/$CuFe_2O_4$) would have restrained polymeric backbone of PANI and volumetric change of $CuFe_2O_4$ during the doping-dedoping and redox transition, respectively. The low charge-transfer resistance (R_{ct}) value of 8.72 Ω is also responsible for conducting the performance of the ternary composite. Ternary GO/PANI/$CuFe_2O_4$ is a superior electrode material for supercapacitor application with longer cyclic stability and high specific energy. From the electrochemical characterizations, it is ensured that the fabricated ternary GO/PANI/$CuFe_2O_4$ composite can be used in fabricating excellent supercapacitors.